Materials Science & Engineering A 702 (2017) 73–80

Contents lists available at ScienceDirect

Materials Science & Engineering A

journal homepage: www.elsevier.com/locate/msea

Impact of cold spraying on microstructure and mechanical properties of optimized friction stir welded AA2024-T3 joint

W.Y. Li[a,*], N. Li[a], X.W. Yang[a], Y. Feng[a], A. Vairis[a,b]

[a] State Key Laboratory of Solidification Processing, Shaanxi Key Laboratory of Friction Welding Technologies, Northwestern Polytechnical University, Xi'an 710072, PR China

[b] Department of Mechanical Engineering, TEI of Crete, Heraklion, Crete 71004, Greece

ARTICLE INFO

Keywords:
Friction stir welding
Cold spraying
Microstructure
Mechanical properties
Residual stresses

ABSTRACT

The tensile properties of friction stir welded AA2024-T3 joints at the rotation speed range of 600–900 rpm and a constant welding speed of 200 mm/min were summarized, finding that the optimized rotation speed is 600 rpm which yield a maximum tensile strength of 420 MPa. Subsequently, an aluminum coating was deposited on the optimized joint surface by cold spraying (CS). The microstructural evolution in the layer near the surface of the coated joint was investigated by a combination of transmission electron microscopy, electron back-scattered diffraction and differential scanning calorimetry. The results show that the CSed joint exhibits significantly enhanced tensile strength, microhardness and fatigue life. This improvement is attributed to refined grains with a higher number of Guinier-Preston-Bagaryatsky (GPB) zones, finer and more S phases, and lower residual stresses due to the heat flow and shot peening effects by the CS on the layer near the surface. CS is shown to be an additional technique to enhance the mechanical properties of FSWed joints whilst providing corrosion protection for them.

1. Introduction

As a promising solid-state joining technique, friction stir welding (FSW) has been applied extensively to join difficult-to-weld light weight components by conventional fusion processes, especially for high-strength aluminum alloys like the 2xxx and 7xxx series [1,2]. However, the intensive frictional heating and mechanical stirring at the stirred zone produced great inhomogeneities in microstructure and mechanical properties across the joint, which obviously caused lower corrosion resistance and mechanical properties than those of the base material (BM) [3–6]. Moreover, the thermal cycle during FSW can result in higher tensile residual stresses in a weld [3]. Their presence is crucial as they significantly affect weld performance [7–9], especially fatigue properties [7,8] and stress corrosion [9]. It is therefore highly significant to find a more efficient method to improve the corrosion performance and mechanical properties of the joints for the further application of FSW technique.

In the past few years, various research efforts have been made to improve either the mechanical properties [10–13] or corrosion resistance [14–19] of the FSWed joints. Enhanced mechanical properties of FSWs could be achieved easily by optimizing welding parameters and tool geometry. Nevertheless, the corrosion resistance of FSWed joints was not significantly modified [20]. With heat treatment (HT), one of the most important methods, the mechanical properties can be effectively improved by adjusting microstructure and releasing residual stresses of the joints [10,11]. However, HT would lead to a high heat input to whole components, and also be limited by the dimensions of components, for example, the large-scale shipbuildings and aircrafte panels [10]. Therefore, many attempts on shot peening have been conducted on the FSWed joints, which displays a significant improvement on mechanical properties of the joints [12,13], but it does not improve microhardness values and is not suitable for processing large-sized materials.

The other big challenge facing in FSW applications is the low corrosion resistance of the weld seam, due to the rotating tool shoulder has damaged the covering pure Al layer [1]. Many studies have shown that the surface coatings could be the best way to protect the weld from the corrosive environment [17–19]. To obtain a good bonding between the protective coating and the weld surface, laser surface melting and micro-arcoxidation etc. have been attempted [17–19]. Although the corrosion resistance were highly improved, an obvious decrease was also widely reported on the mechanical properties of the coated joints caused by the high heat input during the surface coating process. All those reports indicated that it is highly necessary to find an effective

* Corresponding author.
E-mail address: liwy@nwpu.edu.cn (W.Y. Li).

http://dx.doi.org/10.1016/j.msea.2017.07.003
Received 31 May 2017; Received in revised form 30 June 2017; Accepted 1 July 2017
Available online 03 July 2017
0921-5093/

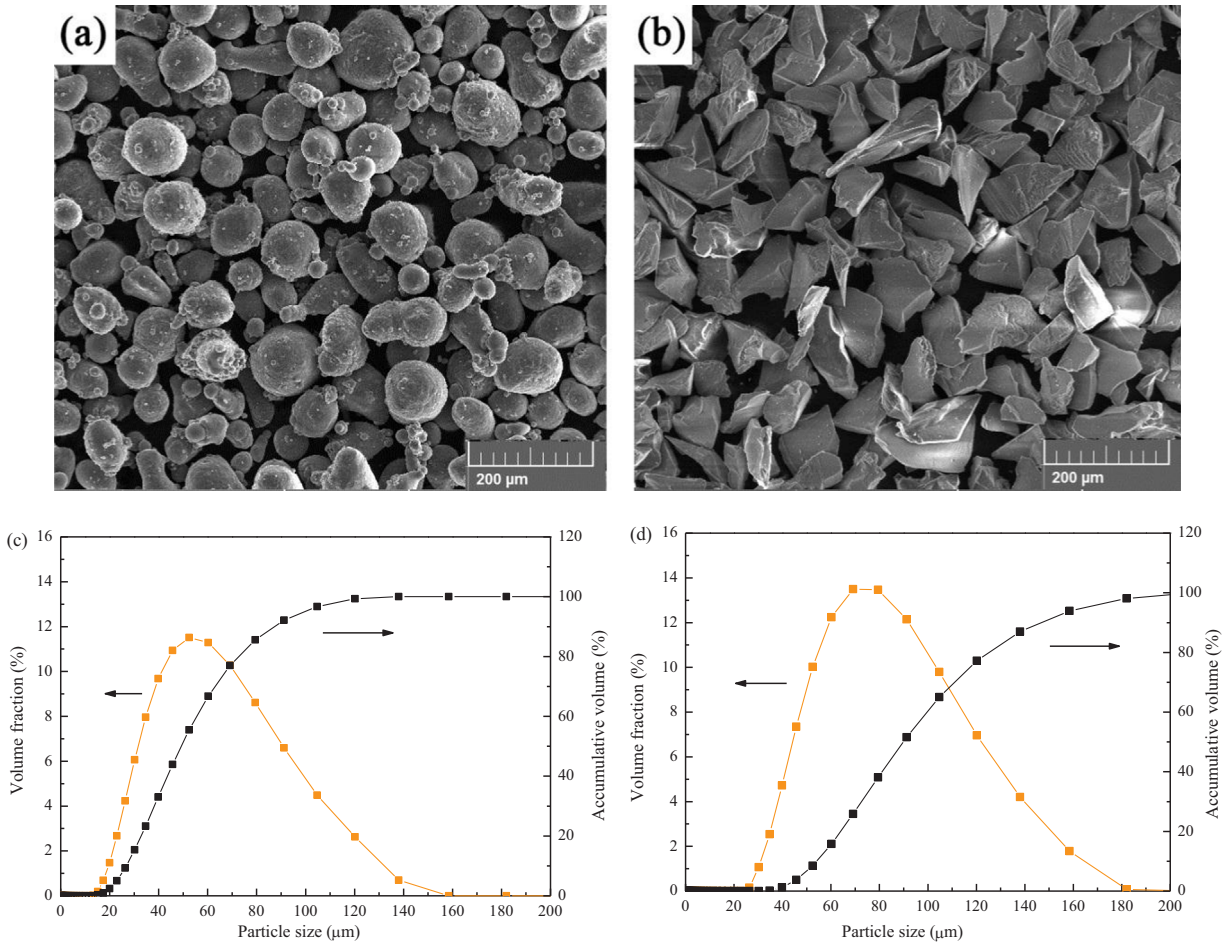

Fig. 1. SEM micrographs and particle size distributions of the powders: (a, c) pure Al powder and (b, d) Al_2O_3 powder.

method to enhance the FSWed joints on both mechanical properties and corrosion resistances.

Cold spraying (CS) as a newly emerging solid-state process, is a powder deposition process characterized by low process temperatures and high-velocity particle impact has received attention [21,22]. Due to these features, the main advantage of CS is that it alleviates the problems associated with high temperature processing of materials, such as oxidation and unfavourable structure changes. Therefore, CSed coatings are used for repair, additive manufacturing and corrosion protection at relatively high deposition rates and low porosity. During CS, the high speed particles accelerated by a gas flow continuously impact the substrate and deform extensively, consequently producing compressive residual stresses in the substrate surface and improving the fatigue performance, similarly to the "shot peening effect (SPE)" [23–25]. It has been shown that the bombardment generated by particles during CS, induces compressive residual stresses near the surface of the substrate, and improves fatigue properties of the substrate [9,26]. Furthermore, the gas is usually preheated to a temperature well below the melting point of the spray material, in order to increase the particle temperature and deformability, similarly to the "heat flow effect (HFE)" [27,28]. In addition, previous results showed that CSed Al-Al_2O_3 coatings on carbon steel and light alloys exhibit excellent corrosion-resistance [29,30]. However, very few studies have been made to evaluate the effect of CSed coating on the microstructure and properties of FSWed joints. In the previous study [31], it is interesting to find that the FSWed joint with a CSed Al coating would exhibit good corrosion resistance and improved mechanical properties. However, in that work [31], the as-FSWed joint was not the optimized one (the tensile strength was only 333 MPa, about 70% of the base metal), one could not clarify the underlying mechanism.

In this study, therefore, the effect of welding parameters (rotation speed) on mechanical properties of FSWed high-strength aluminum alloy joints was demonstrated and then the optimized parameters were chosen for subsequent investigation. The aim is to further enhance the mechanical properties of the FSWed high-strength aluminum alloy joint obtained under the optimized parameters through a CS process and explore the underlying mechanisms via a detailed study of the microstructure and residual stresses before and after coating.

2. Experimental procedure

2.1. Materials and coating preparation

The BM used in the present study is AA2024-T3 alloy sheets. Its heat treatment condition of T3 implies a solution treatment, quenching, predeformation and natural aging. The AA2024-T3 sheets with dimensions of $200 \times 100 \times 3.2$ mm were friction stir butt-welded along the rolling direction by a commercial FSW machine (FSW-RL31-010, Beijing FSW Technology Co., Ltd., PR China). The tool rotation speed were 400 rpm, 600 rpm, 800 rpm, and 900 rpm with a constant welding speed of 200 mm/min according to the previous study [32,33]. The welding tool had a shoulder diameter, probe root diameter and probe length of 10 mm, 3.4 mm and 2.9 mm, respectively. The stir tool was tilted 2.5° (Z-axis) and the plunging depth of the tool shoulder was 0.2 mm.

Commercially available Al and Al_2O_3 powders were used in this study. The Al powder was mixed with 20 vol% Al_2O_3. The Al-Al_2O_3 composite powder was CSed onto the FSWed joint surface using a CS system developed in Xi'an Jiaotong University, China. The driving gas

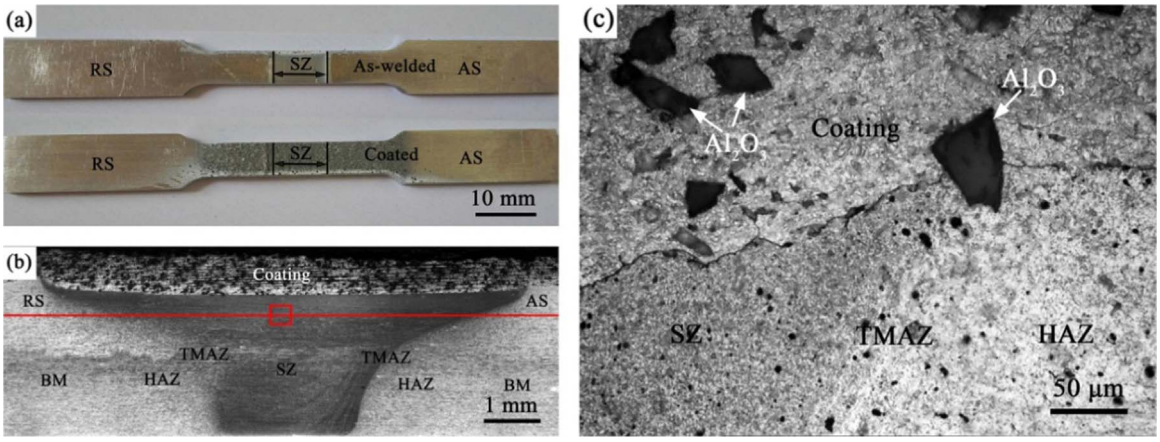

Fig. 2. (a) Tensile samples without (upper) and with (lower) the Al-20 vol% Al_2O_3 coating, (b) cross-sectional OM macrograph of the coating on the joint, (c) higher magnification showing the coating/substrate interface. Note that the location of hardness tests and EBSD measurements in the as-welded and coated joints are in the same position, and are marked by the red line and rectangle.

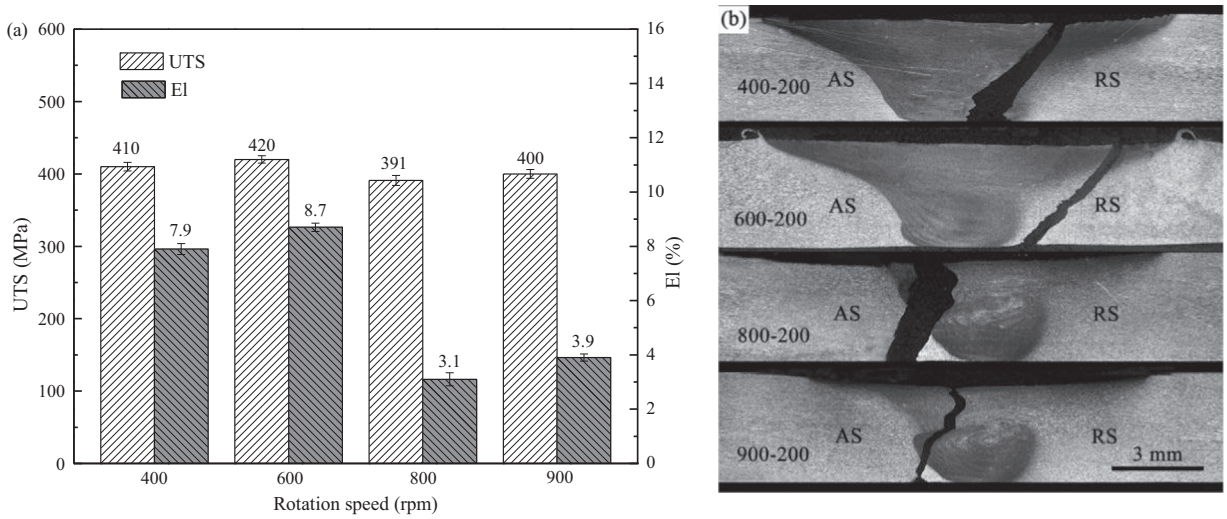

Fig. 3. Tensile test: (a) tensile properties and (b) fracture locations of the joints obtained at different rotation speeds.

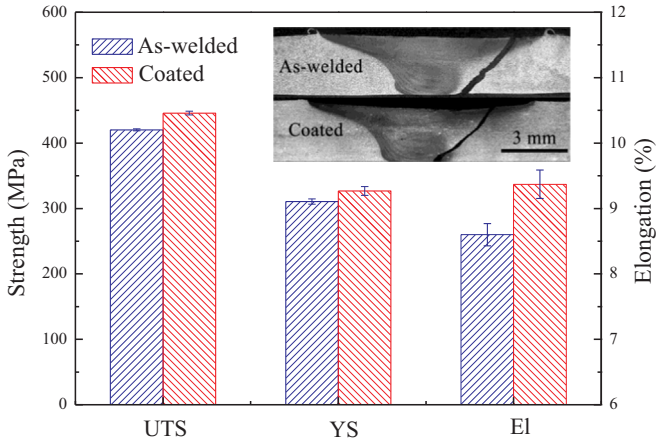

Fig. 4. Tensile properties of as-welded and coated joints.

was nitrogen with an inlet temperature of 450 °C and pressure of 2.8 MPa. The spray gun was held by a robot at a standoff distance of 30 mm and moved across the FSWed joint surface at a transverse speed of 60 mm/s. Prior to deposition, the flash of joints has been removed and sand-blasting was not conducted in order to provide an original joint surface.

2.2. Test methods

The microstructure characterizations were made with an optical microscope (OM), scanning electron microscope (SEM), electron backscattered diffraction (EBSD), transmission electron microscope (TEM) and differential scanning calorimetry (DSC). The residual stresses were measured using X-ray diffraction (XRD) on the orginal joint surface and the coated surface. EBSD specimens were mechanically polished piror to electropolishing. DSC experiments were conducted at a heating rate of 10 °C/min in the temperature range of 50–450 °C. Tensile specimens were machined perpendicular to the FSW direction with a gauge length of 25 mm. Tensile tests were conducted at a cross-head speed of 1 mm/min. The fatigue experiments were implemented with a constant amplitude sinusoidal loading at room temperature. The stress ratio $R = \sigma_{min}/\sigma_{max}$ was set to 0.1 for the stress level of 200 MPa. The test frequency was 20 Hz. Vickers hardness measurements were taken across the joint cross-section under a load of 200 g for 15 s near the surface layer.

2.3. Powder and joint characterization

Fig. 1 shows the morphologies and sizes of the used two powders. The Al powder shows a rounded morphology, not completely spherical in shape with small particles agglomerated on the large ones (Fig. 1a), and the mean particle size is 53 μm (Fig. 1c). The Al_2O_3 particles are

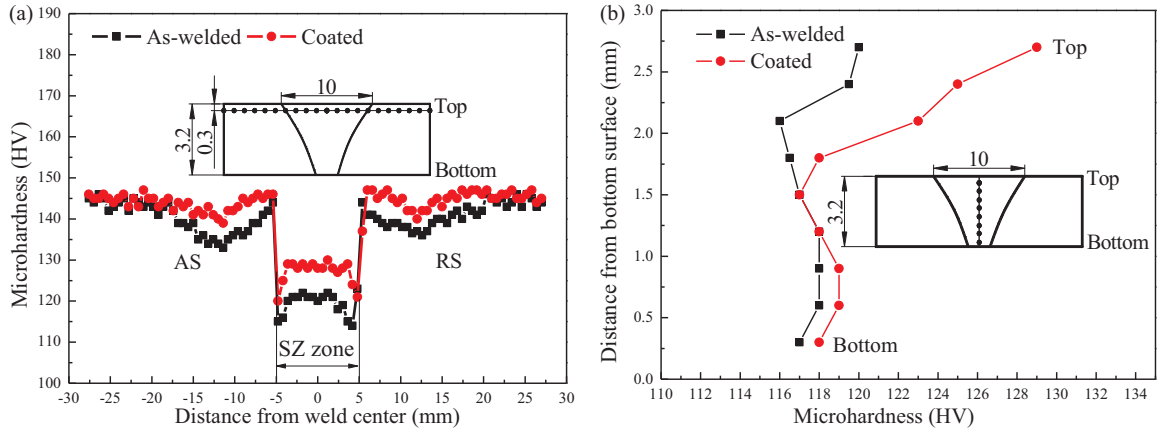

Fig. 5. Hardness profiles (a) across the cross-section of the joint near the top surface and (b) along the thickness in the mid-SZ.

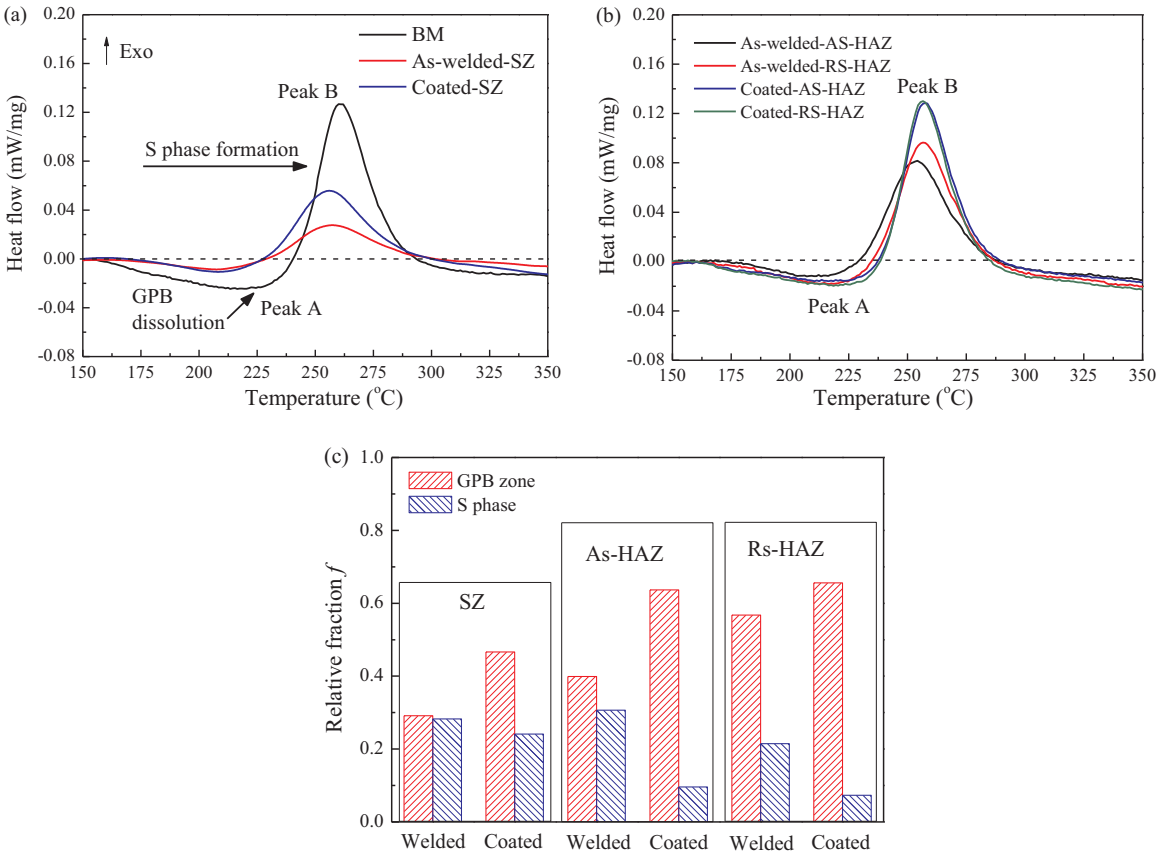

Fig. 6. DSC thermograms of (a) SZs and (b) HAZs under as-welded and coated joint; (c) calculated relative fractions of GPB zone (f_{GPB}) and S phase (f_S).

angular in shape (Fig. 1b) with a mean particle size of 70 μm (Fig. 1d). A view of the Al-20 vol% Al_2O_3 coating on the FSWed AA2024-T3 joint is shown in Fig. 2. It can be seen that the coating width is about 36 mm (Fig. 2a, lower) and its thickness is about 800 μm (Fig. 2b). The coating shows an uniform dispersion of both Al and Al_2O_3 particles. The coating also possesses a relatively dense microstructure with few distinguishable micropores (Fig. 2c) which has been reported by other researchers [34,35]. Moreover, the coating/substrate interface is compact as the joint surface has been subjected to strong particle bombardment during CS. It should be noted that the coating has covered fully all these zones.

3. Results and discussion

3.1. Tensile properties under different welding parameters

Fig. 3a shows the ultimate strength (UTS) and elongation (El) of the joints obtained at different rotation speeds. It can be seen that the maximum UTS of 420 MPa is obtained at the rotation speed of 600 rpm and the maximum El of 8.7 is also obtained at the same rotation speed. This phenomenon may have close connection with the fracture location (Fig. 3b). The fracture location of the FSWed joints located at the weaker regions [36]. The joint welded under the rotation speed of 400 rpm failed at the stir zone (SZ) of the retreating side (RS), but the joint welded under 800 rpm and 900 rpm failed at the SZ of the advancing side (AS). However, the joint welded under 600 rpm failed at the heat-affected zone (HAZ) of the RS and the shear fracture path

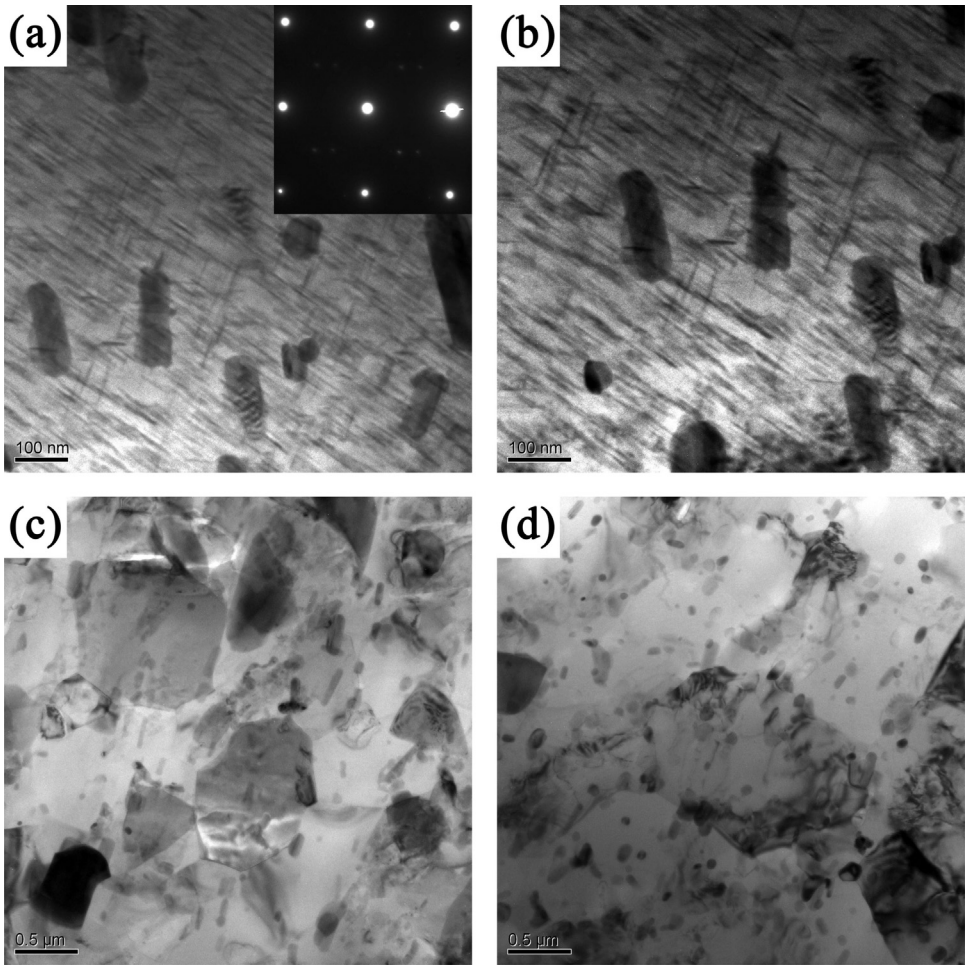

Fig. 7. Bright-field TEM micrographs: HAZ (a, b) and SZ (c, d) under as-welded (a, c) and coated (b, d) joints.

presented a 45° angle to the tensile axis. It was reported that the fracture location of the sound FSWed joints was at the HAZ of the RS [37,38]. Hence, it can be concluded that the rotation speed has a great impact on the tensile properties and the rotation speed of 600 rpm will be used in the subsequent study.

3.2. Mechanical properties

The tensile properties of the as-welded and coated joints are summarized in Fig. 4. The fracture locations of the as-welded and coated joints are shown in the insert of Fig. 4. Fracture has occurred within the HAZ/thermo-mechanically affected zone (TMAZ) of RS. The as-welded joint exhibits lower yield and ultimate tensile strengths (YS and UTS) (310 and 420 MPa) and elongation (El) (8.7%). Coated samples have an increased ultimate tensile strength, yield strength and elongation values, by about 7%, 5% and 9%, respectively. It should be pointed out that the UTS of the coating is around 70 MPa, which is considerably lower than the YS of the as-welded joint. Thus, the coating has been peeled before the fracture of the joint, not showing on the morphology of the fractured joint (Fig. 4 insert). Therefore it is safe to assume that the improvement in tensile properties is not due to the coating itself but to other reasons. When one looks at the hardness profile across the joint surface layer as shown in Fig. 5a, the coated joint shows an significant increase in hardness over the whole joint. A softening region having lower hardness than the BM is produced and the width is about 25 mm, which is not affected by the CSed coating. These hardness profiles are in a good agreement with literature [38,39], where they have a "W"-shaped profile with two lower hardness zones on both the RS and AS sides of the joint. It can be noted that in the two kinds of joints the fracture is almost located at the lower hardness region. Furthermore, the hardness through the joint thickness is affected as well, with an increase of ~ 10 HV for a 0.8 mm length region near the top surface (Fig. 5b).

3.3. Microstructure

In order to fully understand the underlying mechanism, an in depth analysis was conducted, considering microstructural changes and the redistribution of residual stresses. As shown in Fig. 6a and b, DSC analyses of the top surface layer of SZ and the HAZs of both AS and RS indicate the presence of an endothermic and exothermal peak. The endothermic peak A at about 210 °C, corresponds to the dissolution of the Guinier-Preston-Bagaryatsky (GPB) zones, whereas the exothermal peak B at about 270 °C is linked to the precipitation of the S phase (Al_2CuMg) [10,38]. The area under the peak is proportional to the volume fraction of GPB or the S phase present. Consequently, the relative fraction of GPB and S phase initially present in any sample can be calculated by the following equations proposed by Genevois et al. [10], where S stands for the peak area and subscript "0" denotes BM. The calculated f_{GPB} and f_S are shown in Fig. 5c.

$$f_{GPB} = \frac{S_A}{S_{AO}} \tag{1}$$

$$f_S = 1 - \frac{S_B}{S_{BO}} \tag{2}$$

It is clear that when the joint was coated, f_{GPB} increases in both SZ and HAZ. On the contrary, f_S decreases. Depending on the peak temperature, GPB is the main hardening precipitant, and the S phase is either a hardening agent at small sizes or detrimental to hardness at

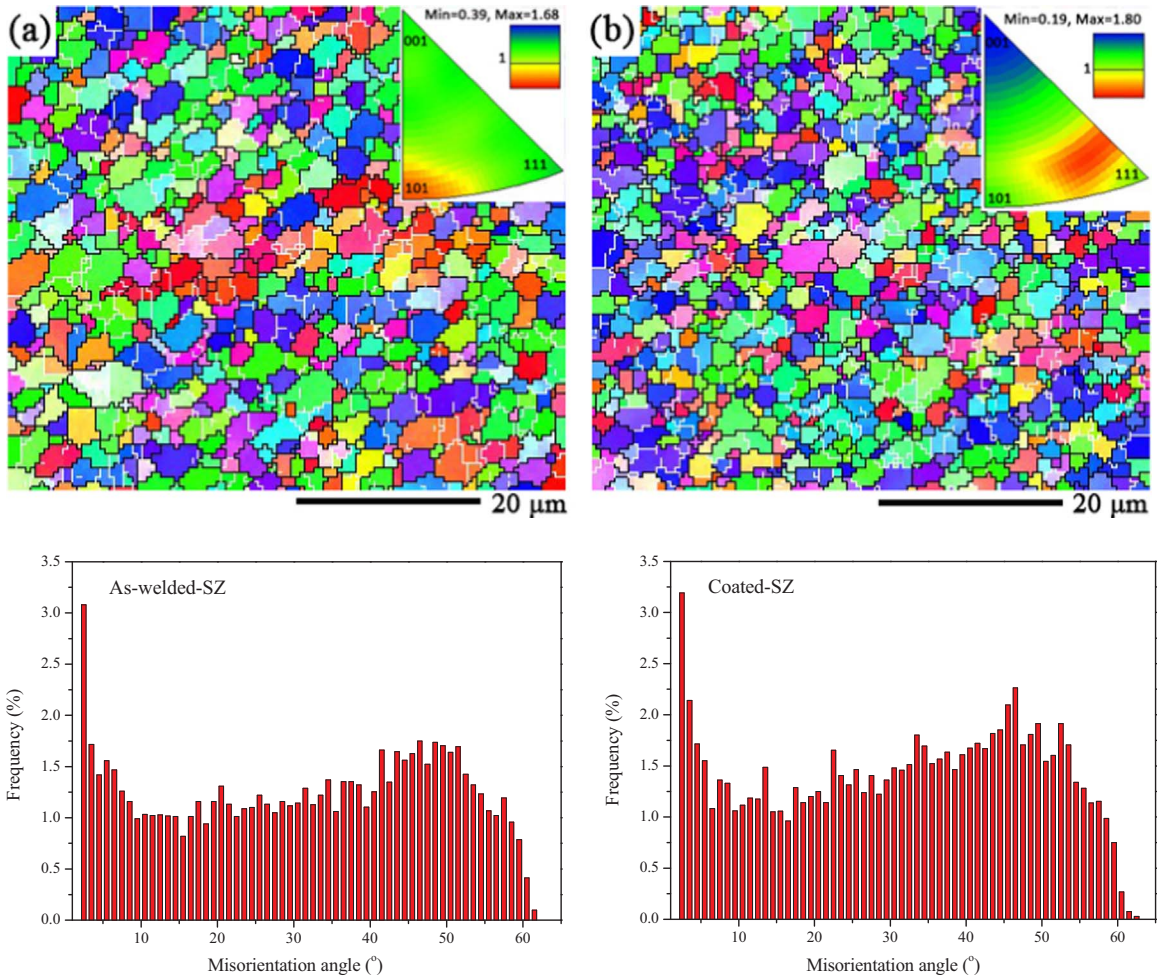

Fig. 8. EBSD maps and misorientation angle distribution in SZs of the joints obtain under (a) as-welded and (b) coated joint.

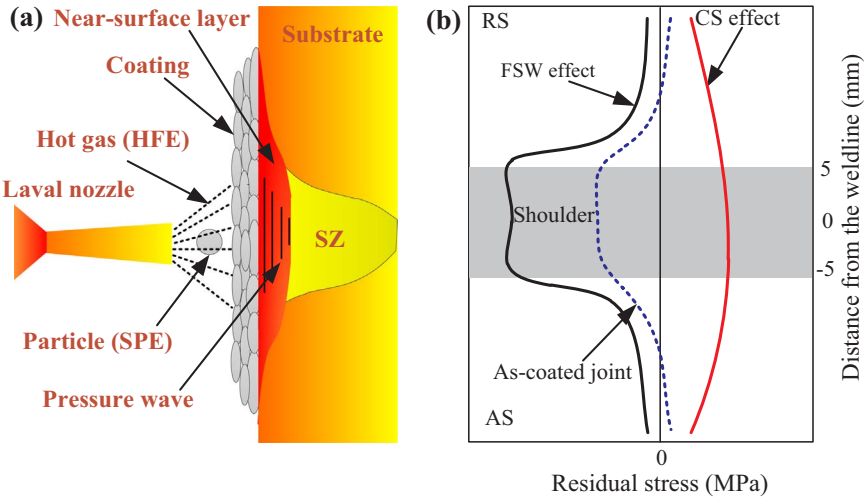

Fig. 9. (a) Effect of CS on the as-welded joint, and (b) residual stress distribution near the joint surface after welding and coating.

large sizes. It is clear that the SZ and HAZ of the coated joint contain more GPB zones which can explain the higher hardness values. The lower temperature during FSW in HAZ effectively prevents the dissolution of GPB zone. The HFE during CS heats up the near-surface layer of the coated joint at a temperature between 200 and 300 °C [27], which improves dramatically the dissolution of the GPB zones both in SZ and HAZ. The more intense the heat input, the higher volume fraction of the GPB zones develops [40]. The corresponding increase in temperature enables the subsequent precipitation of GPB zones which increase hardness [10]. Moreover, under the temperature and sustaining of CS process, the S phase does not become coarser. The coating exerts noticeable influence on the hardness and makes the distributions of GPB and S phases in AS and RS more uniform. Moreover, the SPE during CS may release the residual stresses of the joints, which may also contribute to the hardness improvement. The higher hardness can significantly reduce the formation and growth rate of cracks, and thus improves the joint strength. Hence, the FSWed joints with the coating have better tensile properties than those without coating.

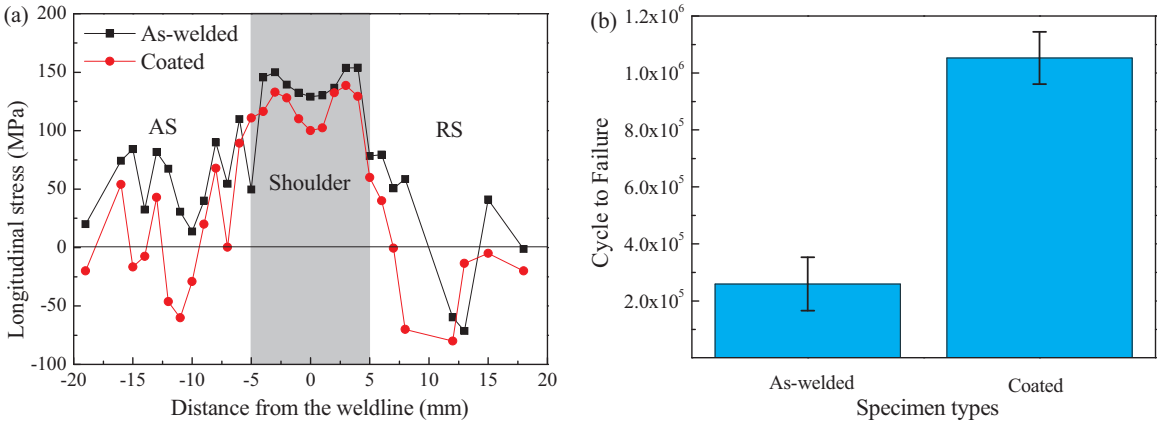

Fig. 10. (a) Comparison of the longitudinal residual stress near the joint surface for the as-welded and coated joints, and (b) fatigue life results at a stress level of 200 MPa.

Fig. 7 displays the bright-field TEM images and associated diffraction patterns of the top surface layer of the SZs and HAZs close to the TMAZ under the as-welded joint and as-coated joint. The microstructure of HAZ in the coated joint was characterized by a higher density of needle-shaped S phases and few coarse Ω phases than that in the as-welded joint. The SZ is the zone undergone the dynamic recrystallisation, with few dislocations left after welding [10]. In the SZ of the as-welded joint, a lot of granule-shaped S phases and few coarse Ω phases are clearly seen due to the short time of high temperature. Furthermore, after being coated, the S phase particles in SZ becomes finer and the fraction seems higher. It is well known that finer S phase in the Al matrix has a pivotal effect in preventing abnormal grain growth and improving the tensile strength by pinning dislocations [5,38,41].

Fig. 8 shows the microstructural characteristics observed by using EBSD in the SZs of the as-welded and coated joints. The size of the equiaxed recrystallized grains in the SZs of the as-welded and coated joints are 2.3 ± 0.1 μm and 1.9 ± 0.1 μm, respectively. The high-angle grain boundaries (HAGBs) (misorientation angle ≥ 15°) of the as-welded and coated joints contribute 57.4% and 67.2% of the total grain boundary length, respectively. Clearly, the SPE during CS has induced plastic deformation in the joint near the surface, producing refined grains, dislocation cell blocks, shot peening strengthening and lower residual stresses [42–45]. It has been reported that heavy plastic deformation may refine grains of metals to make them very strong [46,47]. But there is a limit to grain refinement, and, after a certain limit, straining does not reduce grain size because of the enhanced mobility of grain boundaries. With multi-directional strain paths and high strain rates, grains are effectively rotated, eventually resulting in higher HAGBs. It can be seen, that SPE during CS is more effective in inducing the desired grain refinement while reducing the grain size gradient near the surface of the coated joint. Higher HAGBs and refined grains can hinder dislocations more efficiently due to high stress concentration, with the consequence of enhancing the strain-hardening capacity and improving the ductility of the joint [48].

3.4. Residual stresses on the top surface and fatigue life

The effects of CS on FSWed joints can be schematically shown in Fig. 9a. It can be graphically seen that high-pressure CS systems produce high velocity impact of particles with an intense heat flow to the substrate. It has been verified that the combined effects of HFE and SPE induce multiple changes to microstructure and residual stresses [45], and result in a distinct improvement of mechanical properties of the FSWed joint. Fig. 10a compares the profiles of the longitudinal residual stress near the joint surface between the as-welded and coated joints, which shows that the profile is approximately M-shaped [49]. It indicates that depositing a CSed coating on the joint surface is an significant method in residual stress relaxation. In fact, the SPE effect induces favorable compressive residual stress in the substrate while this high temperature of the HFE effect can have an in-situ annealing role and partially release the stresses induced during spraying [25]. Therefore, it can be concluded that the SPE of CS can modify the residual stress state by positively inducing compressive residual stresses near the surface of the FSWed joint. It is assumed that the peening process is the most significant factor in the accumulation of the compressive peening residual stresses and the thermal effect does not play a notable role in changing the distribution of the induced stresses. Thus, residual stress relaxation at the interface between the FSWed joint and the coating can be observed (Fig. 9b). Fig. 10b displays the fatigue life graphically as histogram plots to highlight the improvement of the coated joints. It indicates that the coated specimens perform better than the as-weld specimens at a stress level of 200 MPa, surviving an average of 1.3E + 06 cycles to failure, an increase of 4 times. Such increase fatigue life on coated specimens may be assisted by the increase in compressive residual stresses imparted by the CS process itself. This has been verified by the positive effect for lower compressive residual stresses aftering CS.

4. Conclusions

In the present work, the optimized rotation speed (600 rpm) was chosen in term of tensile tests. Subsequently, the Al-Al_2O_3 coating was CSed on the surface of the FSWed AA2024-T3 joint obtain under the optimized parameters. The microstructural evolution, microhardness, tensile properties and fatigue properties of the as-welded joint were compared. On the basis of the results the following conclusions are drawn:

(1) The combined effects of HFE and SPE during CS offer a distinct enhancement of microhardness, tensile properties and fatigue properties. The dissolution of GPB zones in the SZ and HAZ is effectively increased under the coated joint. Moreover, the coating makes the distributions of GPB and S phases in AS and RS more uniform.
(2) The S phase particles in the SZ and HAZ of the coates joint become finer and the fraction is higher due to the effect of heat treatment generated by HFE during CS.
(3) The grains in the coated joint are refined compared to those in the as-welded joint. The average grain sizes, estimated by EBSD, are about 2.3 μm and 1.9 μm for SZs in the as-welded and coated joints, respectively.
(4) The coated joint successfully produces superior strength-ductility synergy due to the more HAGBs, refined grains, more GPB zones and lower residual stresses. The average UTS, El and fatigue life of the coated joint increase by 7%, 9% and 4 times, respectively.

Acknowledgements

The authors would like to thank for financial support the National Natural Science Foundation of China (51574196), the 111 Project (B08040), the fund of SAST (SAST2016043) and the National Key Research and Development Program of China (2016YFB0701203).

References

[1] Y.M. Yue, Z.W. Li, S.D. Ji, Y.X. Huang, Z.L. Zhou, Effect of reverse-threaded pin on mechanical properties of friction stir lap welded alclad 2024 aluminum alloy, J. Mater. Sci. Technol. 32 (2016) 671–675.
[2] M. Bahrami, M.F. Nikoo, M.K.B. Givi, Microstructural and mechanical behaviors of nano-SiC-reinforced AA7075-O FSW joints prepared through two passes, Mater. Sci. Eng. A 626 (2015) 220–228.
[3] P.L. Niu, W.Y. Li, Z.H. Zhang, X.W. Yang, Global and local constitutive behaviors of friction stir welded AA2024 joints, J. Mater. Sci. Technol. (2017).
[4] Y. Deng, B. Peng, G.F. Xu, Q.L. Pan, R. Ye, Y.J. Wang, L.Y. Lu, Z.M. Yin, Stress corrosion cracking of a high-strength friction-stir-welded joint of an Al–Zn–Mg–Zr alloy containing 0.25 wt% Sc, Corros. Sci. 100 (2015) 57–72.
[5] E. Bousquet, A. Poulon-Quintin, M. Puiggali, O. Devos, M. Touzet, Relationship between microstructure, microhardness and corrosion sensitivity of an AA 2024-T3 friction stir welded joint, Corros. Sci. 53 (2011) 3026–3034.
[6] A.T. Kermanidis, A. Tzamtzis, An experimental approach for estimating the effect of heat affected zone (HAZ) microstructural gradient on fatigue crack growth rate in aluminum alloy FSW, Mater. Sci. Eng. A 691 (2017) 110–120.
[7] D.R. Ni, D.L. Chen, B.L. Xiao, D. Wang, Z.Y. Ma, Residual stresses and high cycle fatigue properties of friction stir welded SiCp/AA2009 composites, Int. J. Fatigue 55 (2013) 64–73.
[8] G. Biallas, Effect of welding residual stresses on fatigue crack growth thresholds, Int. J. Fatigue 50 (2013) 10–17.
[9] P.S. Prevey, J.T. Cammett, The influence of surface enhancement by low plasticity burnishing on the corrosion fatigue performance of AA7075-T6, Int. J. Fatigue 26 (2004) 975–982.
[10] C. Genevois, A. Deschamps, A. Denquin, B. Doisneau-Cottignies, Quantitative investigation of precipitation and mechanical behaviour for AA2024 friction stir welds, Acta Mater. 53 (2005) 2447–2458.
[11] G. İpekoğlu, G. Çam, Effects of initial temper condition and postweld heat treatment on the properties of dissimilar friction-stir-welded joints between AA7075 and AA6061 aluminum alloys, Metall. Mater. Trans. A 45 (2014) 3074–3087.
[12] O. Hatamleh, Effects of peening on mechanical properties in friction stir welded 2195 aluminum alloy joints, Mater. Sci. Eng. A 492 (2008) 168–176.
[13] G. Liu, S.C. Wang, X.F. Lou, J. Lu, K. Lu, Low carbon steel with nanostructured surface layer induced by high-energy shot peening, Scr. Mater. 44 (2001) 1791–1795.
[14] C.S. Paglia, K.V. Jata, R.G. Buchheit, The influence of artificial aging on the microstructure, mechanical properties, corrosion, and environmental cracking susceptibility of a 7075 friction-stir-weld, Mater. Corros. 58 (2007) 737–750.
[15] S.J. Kalita, Microstructure and corrosion properties of diode laser melted friction stir weld of aluminum alloy 2024 T351, Appl. Surf. Sci. 257 (2011) 3985–3997.
[16] C.S. Paglia, R.G. Buchheit, The influence of a propane gas torch flame post-weld heat treatment on the mechanical and corrosion properties of a 2219-T87 friction stir weld, Weld. Cut. 6 (2007) 96–102.
[17] C. Padovani, A.J. Davenport, B.J. Connolly, S.W. Williams, E. Siggs, A. Groso, M. Stampanoni, Corrosion protection of AA7449-T7951 friction stir welds by laser surface melting with an excimer laser, Corros. Sci. 53 (2011) 3956–3969.
[18] C. Padovani, A.J. Davenport, B.J. Connolly, S.W. Williams, E. Siggs, A. Groso, M. Stampanoni, Corrosion protection of AA2024-T351 friction stir welds by laser surface melting with excimer laser, Corros. Eng. Sci. Technol. 47 (2012) 188–202.
[19] Y. Yang, L. Zhou, Improving corrosion resistance of friction stir welding joint of 7075 aluminum alloy by micro-arc oxidation, J. Mater. Sci. Technol. 30 (2014) 1251–1254.
[20] H.J. Liu, Y.Y. Hu, C. Dou, D.P. Sekulic, An effect of the rotation speed on microstructure and mechanical properties of the friction stir welded 2060-T8 Al-Li alloy, Mater. Charact. 123 (2017) 9–19.
[21] C.J. Huang, W.Y. Li, Y. Feng, Y.C. Xie, M.P. Planche, H.L. Liao, G. Montavon, Microstructural evolution and mechanical properties enhancement of a cold-sprayed Cu Zn alloy coating with friction stir processing, Mater. Charact. 125 (2017) 76–82.
[22] S. Dosta, G. Bolelli, A. Candeli, L. Lusvarghi, I.G. Cano, J.M. Guilemany, Plastic deformation phenomena during cold spray impact of WC-Co particles onto metal substrates, Acta Mater. 124 (2017) 173–181.
[23] R. Ghelichi, S. Bagherifard, D. MacDonald, I. Fernandez-Pariente, B. Jodoin, M. Guagliano, Experimental and numerical study of residual stress evolution in cold spray coating, Appl. Surf. Sci. 288 (2014) 26–33.
[24] S. Rech, A. Trentin, S. Vezzù, J.G. Legoux, E. Irissou, M. Guagliano, Influence of pre-heated Al 6061 substrate temperature on the residual stresses of multipass Al coatings deposited by cold spray, J. Therm. Spray. Technol. 20 (2011) 243–251.
[25] K. Spencer, V. Luzin, N. Matthews, M.X. Zhang, Residual stresses in cold spray Al coatings: the effect of alloying and of process parameters, Surf. Coat. Technol. 206 (2012) 4249–4255.
[26] C.W. Ziemian, M.M. Sharma, B.D. Bouffard, T. Nissley, T.J. Eden, Effect of substrate surface roughening and cold spray coating on the fatigue life of AA2024 specimens, Mater. Des. 54 (2014) 212–221.
[27] W.Y. Li, S. Yin, X.P. Guo, H.L. Liao, X.F. Wang, C. Coddet, An investigation on temperature distribution within the substrate and nozzle wall in cold spraying by numerical and experimental methods, J. Therm. Spray. Technol. 21 (2012) 41–48.
[28] M. Fukumoto, H. Wada, K. Tanabe, M. Yamada, E. Yamaguchi, A. Niwa, M. Sugimoto, M. Izawa, Effect of substrate temperature on deposition behavior of copper particles on substrate surfaces in the cold spray process, J. Therm. Spray. Technol. 16 (2007) 643–650.
[29] F.S. da Silva, J. Bedoya, S. Dosta, N. Cinca, I.G. Cano, J.M. Guilemany, A.V. Benedetti, Corrosion characteristics of cold gas spray coatings of reinforced aluminum deposited onto carbon steel, Corros. Sci. 114 (2017) 57–71.
[30] D. Dzhurinskiy, E. Maeva, E. Leshchinsky, R.G. Maev, Corrosion protection of light alloys using low pressure cold spray, J. Therm. Spray. Technol. 21 (2012) 304–313.
[31] W.Y. Li, R.R. Jiang, C.J. Huang, Z.H. Zhang, Y. Feng, Effect of cold sprayed Al coating on mechanical property and corrosion behavior of friction stir welded AA2024-T351 joint, Mater. Des. 65 (2015) 757–761.
[32] Z.H. Zhang, W.Y. Li, J.J. Shen, Y.J. Chao, J.L. Li, Y.E. Ma, Effect of backplate diffusivity on microstructure and mechanical properties of friction stir welded joints, Mater. Des. 50 (2013) 551–557.
[33] Z.H. Zhang, W.Y. Li, Y. Feng, J.L. Li, Y.J. Chao, Global anisotropic response of friction stir welded 2024 aluminum sheets, Acta Mater. 92 (2015) 117–125.
[34] K. Spencer, D.M. Fabijanic, M.X. Zhang, The use of Al–Al_2O_3 cold spray coatings to improve the surface properties of magnesium alloys, Surf. Coat. Technol. 204 (2009) 336–344.
[35] E. Irissou, J.G. Legoux, B. Arsenault, C. Moreau, Investigation of Al-Al_2O_3 cold spray coating formation and properties, J. Therm. Spray. Technol. 16 (2007) 661–668.
[36] R.S. Mishra, Z.Y. Ma, Friction stir welding and processing, Mater. Sci. Eng. R 50 (2005) 1–78.
[37] Z.H. Zhang, W.Y. Li, Y. Feng, J.L. Li, Y.J. Chao, Improving mechanical properties of friction stir welded AA2024-T3 joints by using a composite backplate, Mater. Sci. Eng. A 598 (2014) 312–318.
[38] Z. Zhang, B.L. Xiao, Z.Y. Ma, Hardness recovery mechanism in the heat-affected zone during long-term natural aging and its influence on the mechanical properties and fracture behavior of friction stir welded 2024Al–T351 joints, Acta Mater. 73 (2014) 227–239.
[39] B. Malard, F. De Geuser, A. Deschamps, Microstructure distribution in an AA2050 T34 friction stir weld and its evolution during post-welding heat treatment, Acta Mater. 101 (2015) 90–100.
[40] V. Dixit, R.S. Mishra, R.J. Lederich, R. Talwar, Influence of process parameters on microstructural evolution and mechanical properties in friction stirred Al-2024 (T3) alloy, Sci. Technol. Weld. Join. 14 (2009) 346–355.
[41] Z.L. Hu, X.S. Wang, S.J. Yuan, Quantitative investigation of the tensile plastic deformation characteristic and microstructure for friction stir welded 2024 aluminum alloy, Mater. Charact. 73 (2012) 114–123.
[42] M.R. Rokni, C.A. Widener, V.K. Champagne, S.R. Nutt, The effects of heat treatment on 7075 Al cold spray deposits, Surf. Coat. Technol. 310 (2016) 278–285.
[43] S. Yin, X.F. Wang, X.K. Suo, H.L. Liao, Z.W. Guo, W.Y. Li, C. Coddet, Deposition behavior of thermally softened copper particles in cold spraying, Acta Mater. 61 (2013) 5105–5118.
[44] V. Luzin, K. Spencer, M.X. Zhang, Residual stress and thermo-mechanical properties of cold spray metal coatings, Acta Mater. 59 (2011) 1259–1270.
[45] X. Wu, N. Tao, Y. Hong, B. Xu, J. Lu, K. Lu, Microstructure and evolution of mechanically-induced ultrafine grain in surface layer of AL-alloy subjected to USSP, Acta Mater. 50 (2002) 2075–2084.
[46] X.C. Liu, H.W. Zhang, K. Lu, Strain-induced ultrahard and ultrastable nanolaminated structure in nickel, Science 342 (2013) 337–340.
[47] L. Lu, Y. Shen, X. Chen, L. Qian, K. Lu, Ultrahigh strength and high electrical conductivity in copper, Science 304 (2004) 422–426.
[48] Y.H. Zhao, Y.T. Zhu, E.J. Lavernia, Preparation of nanostructured materials having improved ductility, Adv. Eng. Mater. 12 (2010) 769–788.
[49] X.X. Zhang, D.R. Ni, B.L. Xiao, H. Andrä, W.M. Gan, M. Hofmann, Z.Y. Ma, Determination of macroscopic and microscopic residual stresses in friction stir welded metal matrix composites via neutron diffraction, Acta Mater. 87 (2015) 161–173.